Geologica Acta, Vol.7, Nº 4, December 2009, 399-412
DOI: 10.1344/104.000001446
Available online at www.geologica-acta.com

geologica acta

Tourmaline $^{40}Ar/^{39}Ar$ chronology of tourmaline-rich rocks from Central Iberia dates the main Variscan deformation phases

F. BEA [1] **A. PESQUERA** [2] **P. MONTERO** [1] **J. TORRES-RUIZ** [1] **and P. P. GIL-CRESPO** [2]

[1] **Department of Mineralogy and Petrology**
Campus Fuentenueva, Universidad de Granada, 18002 Granada, Spain. Bea E-Mail: fbea@ugr.es

[2] **Department of Mineralogy and Petrology**
Campus Leioa, University of the Basque Country, 48080 Bilbao, Spain

ABSTRACT

During crustal thickening, metapelites taken to depth release boron-bearing hydrothermal fluids because of progressive heating and dehydration. These fluids swiftly percolate upwards, especially if the crust is being actively deformed, to form tourmaline where the PT conditions and the chemical composition of the host-rock are favorable. The age of the so-formed tourmaline would record the age of the upward admittance of B-bearing fluids and, presumably, the age of the deformation. This process has been documented in the Martinamor Antiform of Central Iberia, a region where tourmaline-bearing rocks are particularly abundant. Metasomatic tourmaline from the Late Cambrian San Pelayo orthogneisses (zircon U-Pb age of 496 ± 5 Ma) yielded $^{40}Ar/^{39}Ar$ plateau ages at 370 ± 5 Ma and 342 ± 5 Ma. The first value represents the crystallization age of the tourmaline and is so far the most precise estimation of the age of crustal thickening in Central Iberia (D1). The second value reflects a partial loss of Ar caused by the second deformation phase (D2). Tourmaline from mylonitized and folded tourmalinites developed above D2 shear zones yield perturbed spectra with mean "plateau" ages of 347 ± 9 Ma and 342 ± 9 Ma which may represent either the resetting of older tourmaline or the formation of new tourmaline by focused boron metasomatism. After the metamorphic peak and simultaneously with the emplacement of the main granitoids of the Avila Batholith (310-315 Ma), another episode of boron metasomatism precipitated a new generation of tourmaline, which appears either concentrated in fine-layered tourmalinites (318 ± 2 Ma) or disseminated within Ediacaran-Cambrian metasediments (316 ± 2 Ma). The source of boron was the breakdown of previously formed tourmaline during melting reactions. Lastly, tourmaline from a leucogranitic body yielded a saddle-shaped age spectrum with a minimum age of ca. 296 Ma, roughly coeval with the youngest leucogranites. Although further work is required, our results suggest that tourmaline can be a useful chronological marker for dating deformation and magmatism.

KEYWORDS | **Tourmaline. $^{40}Ar/^{39}Ar$ dating. Deformation. Iberia. Boron. Metasomatism.**

INTRODUCTION

The precise age of the Variscan crustal stacking in the Central Iberian Zone (Fig. 1), which followed the closure of the Galician-South Brittany ocean during the Late Devonian or the Early Carboniferous (Matte, 2001), is not yet well-known because of the lack of syn-collisional magmatic rocks. In the north of this area, Dallmeyer et al. (1997) determined $^{40}Ar/^{39}Ar$ ages in muscovites from low-grade greenschist to amphibolite facies metasediments at 359 Ma which these authors interpret as reflecting the first deformation phase. In the center and the South, the oldest precisely determined Variscan ages correspond to a small zircon population at ca. 350 Ma in the Peña Negra migmatites of the Avila Batholith (Montero et al., 2004). This date, however, does not represent the age of collision, because the thickened Central Iberian crust required some tens of millions of years of thermal maturation before undergoing anatexis (Bea et al., 2003). A better estimate of the age of the collision could be obtained from any mineral formed during, or immediately after, crustal thickening. Tourmaline seems, in this case, a good candidate because the pre-Variscan crust of Central Iberia was mostly metapelitic, as evidenced by geophysical and xenolith data (Bea et al., 1999; Villaseca et al., 1999 and references therein mentioned), and metapelites taken to depth will have released boron into the dehydration vapor phase (e.g., Moran et al., 1992) which will then migrate through the deforming crust to precipitate tourmaline wherever they permeate rocks with a favorable bulk-composition.

Radiometric dating of tourmaline is not often performed and has occasionally yielded controversial results (e.g., Frei and Pettke, 1997; Richards and Wagner, 1997). To our knowledge, tourmaline has been successfully dated by Pb-Pb (Frei and Pettke, 1996; Kudryashov et al., 2004), Rb-Sr (Chen et al., 1996), Sm-Nd (Anglin et al., 1996) and, especially, K-Ar and $^{40}Ar/^{39}Ar$ (Fitch and Miller, 1972; Allen, 1991; Andriessen et al., 1991) (but,

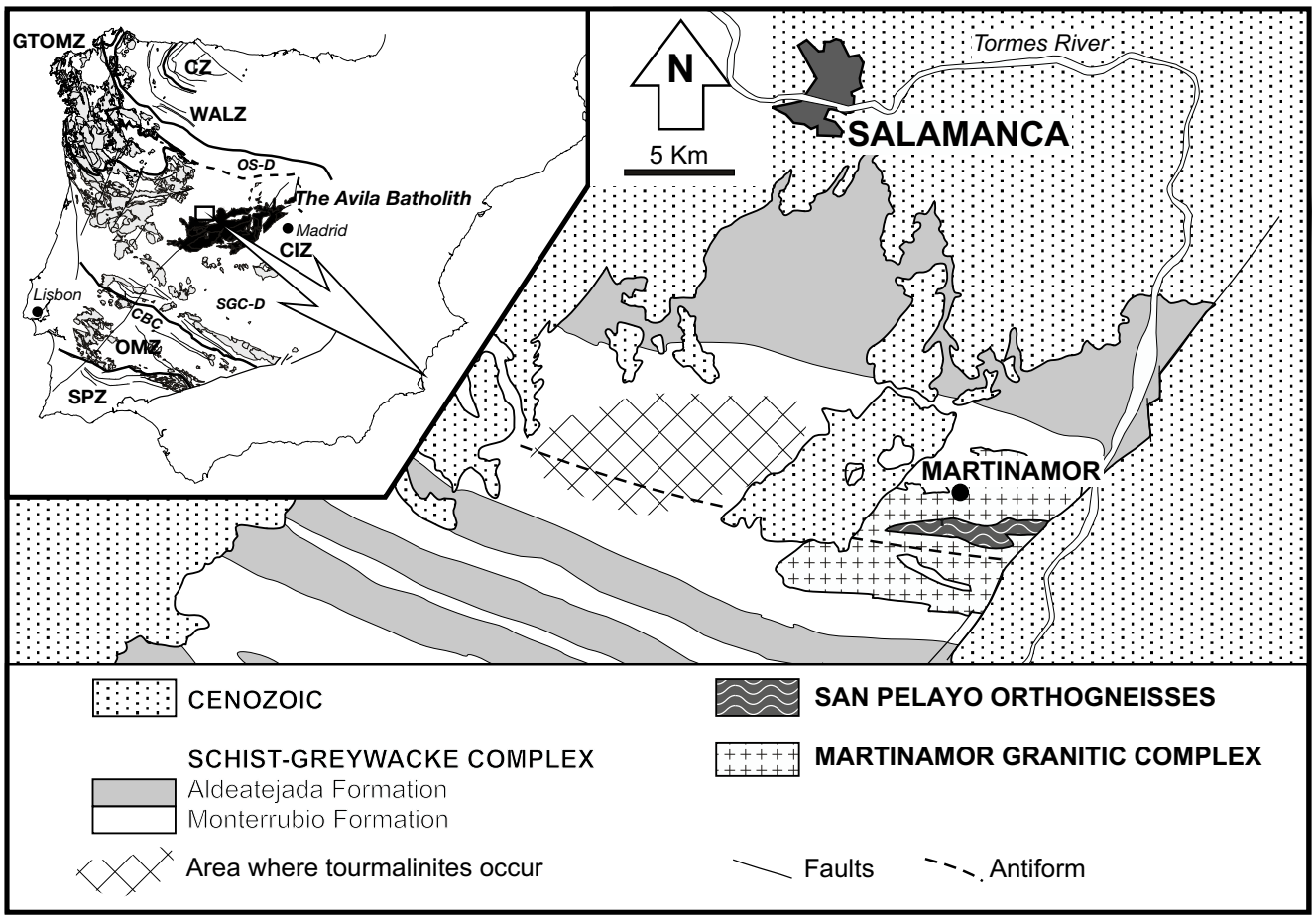

FIGURE 1 | **Geological sketch of the Martinamor antiform. In the large-scale map the zones of the Iberian massif are CZ: Cantabrian Zone; WALZ: Western-Astur Leonian Zone; GTOMZ: Galicia Tras-os-Montes Zone; CIZ: Central Iberian Zone; OMZ: Ossa Morena Zone; SPZ: South Portuguese Zone. In the CIZ, OS-D and SGC-D refer to the Ollo de Sapo Domain and Schist Greywacke Complex Domain, respectively.**

see Villa, 1990). Among these options, we have chosen the laser-step heating $^{40}Ar/^{39}Ar$ method, because preliminary LA-ICPMS analyses of the studied tourmalines have revealed low elemental abundances of Pb, Sm and Nd, and small variations of Rb/Sr and Sm/Nd (authors' unpublished data). Considering that tourmaline is resilient to alteration and metamorphism almost up to anatexis (Von Goerne et al., 1999; Kawakami, 2001) and has an Ar closure temperature that, despite the lack of detailed experimental studies, seems higher than hornblende (Andriessen et al., 1991), we considered it possible that tourmaline could still keep a record of its primary crystallization age despite the protracted post-collisional thermal history of the orogen.

The present study is an attempt to date tourmaline from a variety of tourmaline-rich rocks in the Martinamor Antiform, an area of Central Iberia where these rocks are particularly abundant (Fig. 1). Using prompt-gamma NAA, we first determined the concentration of B in low-grade upper crustal metapelites from the Monterrubio and Aldeatejada formations (Fig. 1) and lower crustal metapelitic xenoliths from the neighboring central Spain camptonites (Bea et al., 1999) and found an intense boron depletion of the Central Iberian lower crust during Variscan times, which we suggest was the source of B that ultimately led to the formation of collision-related metasomatic tourmaline. Then, we studied the San Pelayo orthogneiss, composed of pre-Variscan tourmaline-bearing gneissose granites, and several spatially associated tourmaline-rich rocks that are present in Upper Proterozoic metasediments. Using zircon U-Pb ion microprobe and laser ablation ICP-MS dating, we determined the crystallization age of the protolith of the San Pelayo gneisses as Late Cambrian. Subsequently, with $^{40}Ar/^{39}Ar$ dating we showed that the tourmaline of the orthogneiss is considerably younger (Late Devonian) and the tourmaline of the surrounding tourmaline-rich rocks is Carboniferous. From these results, we discuss (1) whether the $^{40}Ar/^{39}Ar$ dates recorded by tourmaline represent the age of the Variscan deformation phases in Central Iberia, and (2) the possible mechanisms which may lead to the formation of collision-related tourmaline.

GEOLOGICAL SETTING

The Central Iberian Zone (Martínez Catalán et al., 2004, and references therein mentioned) consists of Proterozoic and lower Paleozoic metasediments and orthogneisses, intruded by numerous late-Variscan granitoids. It comprises two domains (Fig. 1): To the North is the narrow Ollo de Sapo (OS) Domain, characterized by abundant Cambrian-Ordovician metavolcanites and metagranites; to the South, the broad Schist Graywacke Complex (SGC) Domain occurs, characterized by a large Ediacaran-Cambrian metasedimentary formation (Díaz Montes et al., 2004). This, in its northern part, hosts several small plutons of pre-Variscan gneissic granites, such as the San Pelayo orthogneiss of the Martinamor Antiform, situated in the northern periphery of the large Avila Batholith (Fig 1).

The Variscan deformation in Central Iberia may be summarized as follows: the first phase (D1) thickened the crust to ~50 km (Bea et al., 2003). Thickening was mainly caused by the underthrusting of crustal units from the Ossa Morena Zone (Fig. 1) beneath Central Iberia along the Coimbra-Badajoz-Córdoba Shear Zone (Simancas et al., 2003; Azor et al., 2004). In the Martinamor Antiform, D1 caused isoclinal or slightly asymmetric folds with subvertical axial plane trending NW-SW accompanied by a subvertical penetrative schistosity. The age of this event, not yet well-known, has been diversely estimated from Late Devonian to Early Carboniferous. The second deformation phase (D2) was related to the protracted extensional collapse of the orogen. In the Martinamor Antiform, the effects of D1 are significantly masked by D2, the structural features of which are closely related to the metamorphic zonation. D2 caused isoclinal to sheath folds with a strong, locally mylonitic, subhorizontal fabric (Díez Balda, 1986). The age of D2 for this area can be estimated from the syn-kinematic Cespedosa granite, neighboring the San Pelayo orthogneiss, which has been dated by Rb-Sr at 344 ± 5 Ma (Bea et al., 1999), a value that fully agrees with the ca. 340-345 Ma reported for muscovite developed on D2 foliation in low-grade metapelites from the OS Domain ($^{40}Ar/^{39}Ar$, Dallmeyer et al., 1997). The last Variscan deformation phase (D3) produced systems of small localized subvertical shear zones that affected the ca. 295 Ma granites (Bea et al., 1994).

The Variscan metamorphism followed a clockwise P-T path that in this area reached its thermal maximum at 3-4 kbar and 650-700 °C (Díez Balda et al., 1995). The time of the metamorphic peak in this region has not yet been established; however, by analogy with the neighboring anatectic complexes of the Avila batholith, we estimate that it was at ca. 332-325 Ma (the most frequent Variscan age recorded by neoformed zircons of migmatites, see Montero et al., 2004). More details about the structural and metamorphic evolution of this region can be found in Díez Balda (1986) and Díez Balda et al. (1995).

In the Martinamor antiform, the SGC consists of two formations, Monterrubio, composed of metapsammitic, metapelitic and calc-silicate metasediments, and Aldeatejada, chiefly composed of metapelites (Díez Balda, 1986). The granitic rocks of the Martinamor antiform crop out

within the Monterrubio Formation, mainly in the core of the antiform and in the eastern part of the area. They include two groups (Fig. 1): the pre-Variscan San Pelayo orthogneisses, formerly considered as Cadomian (Díez Balda et al., 1995), and the late-Variscan Martinamor Complex. The tourmaline-bearing leucogranites of the Martinamor Complex crop out as lenticular or sheet-like bodies (up to ~1 km across) that are embedded within the metasedimentary sequence. They have sharp to interleaved, or transitional boundaries with the orthogneisses which show evidence of incipient migmatization. Furthermore, tourmaline-rich rocks are widespread minor lithologies within the Martinamor antiform. They occur in the Monterrubio Formation as small discontinuous stratiform bodies within metasediments from the biotite-garnet zone to sillimanite zone (Fig. 1).

PETROGRAPHY AND MINERAL CHEMISTRY OF TOURMALINE-BEARING ROCKS

Most rocks of the Martinamor antiform contain tourmaline. It is present as the principal Fe-Mg silicate in the tourmalinites and as an abundant accessory within the metasediments, the pre-Variscan San Pelayo orthogneisses, and the Variscan leucogranites, pegmatites and quartz veins. Tourmalinites are fine grained (<1 mm) dark brown to black rocks with variable amounts of tourmaline (15-20% to as much as 90%), commonly characterized by a prominent layering in which fine-scale tourmaline-rich laminae alternate with quartz-rich laminae (Fig. 2A). Besides tourmaline, they contain abundant quartz and variable amounts of plagioclase, muscovite and biotite, with apatite and rutile as the main accessory minerals. At several localities, tourmalinites were deformed and recrystallized during D2 as revealed by: 1) different styles of folding and overprinting relations between foliations (Fig. 2B), where tourmaline-rich layers defining an S1 foliation are crenulated by S2; 2) mylonites with a well developed foliation and stretching lineation, which show σ- and δ-type tourmaline porphyroclasts (Fig. 2C, D), and even more complex porphyroclasts displaying deflection-fold and "millipede" microstructures (Pesquera et al., 2005); 3) boudinage of the tourmaline-rich layers and crystals; 4) fibrous and stretching veins (Fig. 2E); 5) crystalline bending, undulate extinction, subgrains and granoblastic textures (Fig. 2D). In thin section, tourmaline grains commonly display a weak zonation with gradational changes in color from core (greenish to reddish-brown) to rim (yellowish-brown). Overall, the tourmaline compositions range from schorl to dravite with Mg/(Mg + Fe) = 0.4-0.7 and $^{x}\chi/(^{x}\chi + Na) = 0.15\text{-}0.52$, where $^{x}\chi$ represents X-site vacancy.

The San Pelayo orthogneiss is composed of two micas ± tourmaline (up to 3 vol.%) in which the regional foliation wraps around the feldspar megacrysts. Tourmaline occurs either as pale-green to green, very fine to medium-grained, subhedral to anhedral grains, forming irregularly shaped clusters associated with quartz and feldspar, or as porphyroclasts (<5 mm) surrounded by the regional foliation defined by the micas and feldspars. Small biotite crystals may appear partially or completely enclosed by tourmaline. The compositional range is narrower than in tourmalinites, with Mg/(Mg + Fe) = 0.55-0.63 and $^{x}\chi/(^{x}\chi + Na) = 0.19\text{-}0.35$.

In the Martinamor leucogranites, tourmaline appears as black, fine to medium-grained crystals either individually disseminated through the rock groundmass or forming ovoidal or lenticular aggregates (<1 cm). Under the microscope, tourmaline crystals are unzoned or weakly zoned with euhedral to anhedral shapes, and are typically embayed by quartz ± feldspar. Pleochroism varies from pale or bluish-green to green. Small euhedral grains may be enclosed by muscovite and garnet. In granitic rocks the tourmaline compositions plot in the schorl field with Mg/(Mg + Fe) and $^{x}\chi/(^{x}\chi + Na)$ ratios of 0.23-0.46 and 0.29-0.52, respectively.

A detailed description of the field relationships, petrography and composition of the tourmaline-rich rocks can be found in Pesquera et al. (2005).

SAMPLES AND METHODS

For this work, we collected six representative samples of tourmaline-bearing rocks: a fine-layered tourmalinite (Fig. 2A), a folded tourmalinite (Fig. 2B), a mylonitized tourmalinite (Fig. 2C), a tourmaline-bearing psammitic-pelitic metasediment, a sample from the San Pelayo orthogneiss (Fig. 2F), and a late-tectonic leucogranite. Tourmaline separates were prepared using the procedure of Pesquera and Velasco (1997). Single tourmaline crystals of 0.15-0.35 mm in size were optically checked with a binocular microscope. Impure grains were removed by hand picking and the rest were split into two fractions. One fraction was finely ground and examined by X-ray diffraction, to check purity. The other was used for $^{40}Ar/^{39}Ar$ dating. In all cases the purity of the tourmaline separates was estimated to be 100%.

Tourmaline samples were analyzed by IR-laser stepwise heating techniques. Argon isotope ratios were measured on a VG 5400Ar mass spectrometer at the Guangzhou Institute of Geochemistry. Tourmaline samples and a monitor standard DRA1 (sanidine with an age of 25.26 ± 0.07 Ma, Wijbrans et al., 1995) were irradiated at the 49-2 reactor in Beijing for 55 hrs. Correction factors for interfering argon isotopes derived from Ca and K

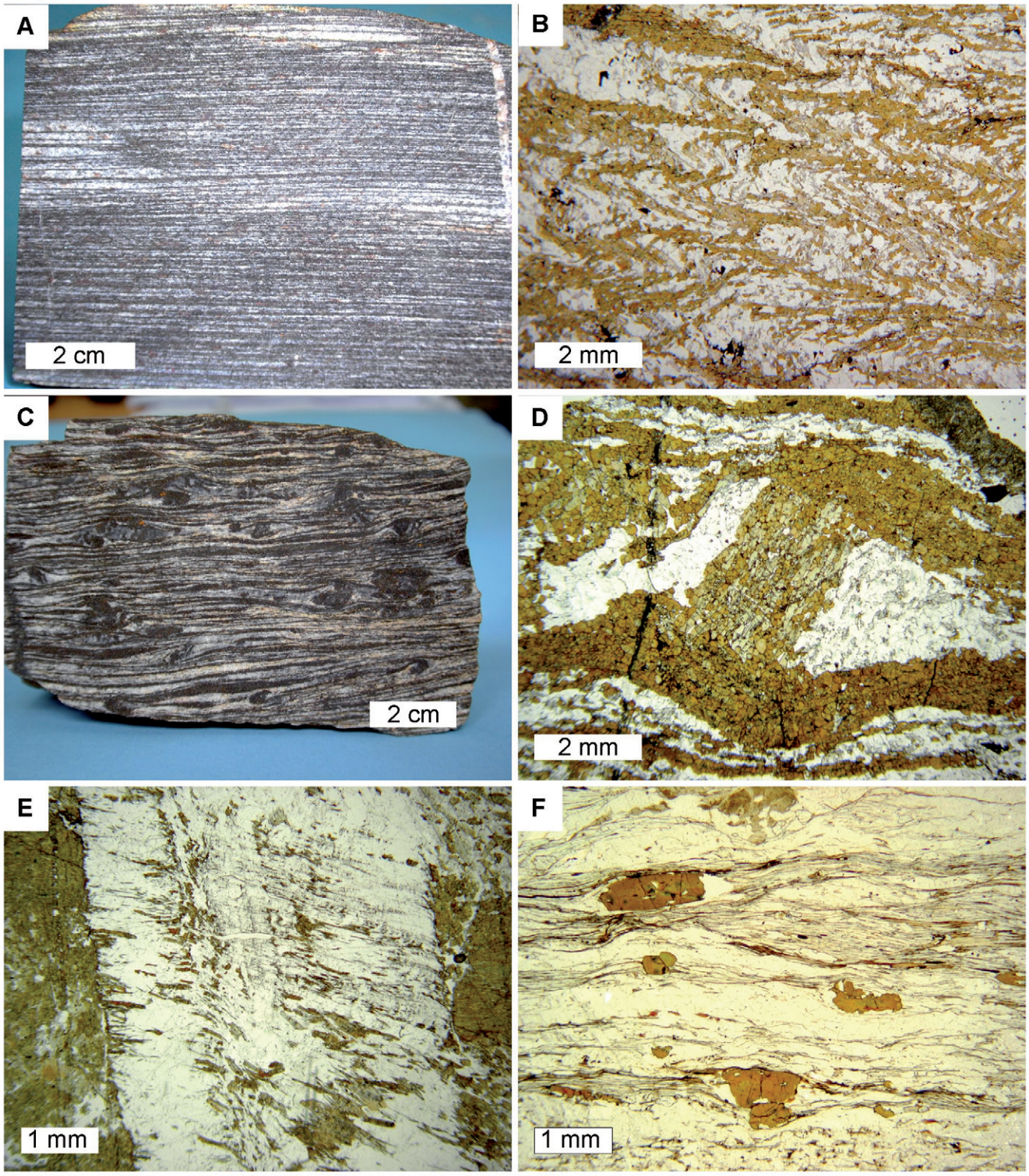

FIGURE 2 | **Hand-sample photographs and photomicrographs of tourmaline-rich rocks from the Martinamor area, Central Iberian Zone. A) Layered quartz-tourmaline tourmalinite. B) Crenulation cleavage in tourmalinite with symmetric microfolds; the foliation is defined by cleavage domains (microfold flanks) and microlithons (fold hinge quartz-rich areas), plane-polarized light. C) Mylonitic tourmalinite displaying complex tourmaline porphyroclasts (overturned-type, tadpole-type, and δ-type objects) in a section perpendicular to foliation and parallel to the stretching lineation. D) Detail of a tourmaline porphyroclast wrapped by the mylonitic foliation (S2), which consists of an aggregate of numerous, very small crystals defining a S1 foliation, plane-polarized light. E) Syntaxial tourmaline-quartz vein in tourmalinite, where the formation of tourmaline can keep pace with the multistage crack opening and sealing. Note the presence of inclusion bands parallel to the vein walls; plane-polarized light. F) Biotite-muscovite orthogneiss in which the foliation defined by micas and lenses of quartz and feldspar wrap around tourmaline porphyroclasts, plane-polarized light.**

are: $(^{39}Ar/^{37}Ar)Ca = 8.984 \times 10^{-4}$, $(^{36}Ar/^{37}Ar)Ca = 2.673 \times 10^{-4}$ and $(^{40}Ar/^{39}Ar)K = 5.97 \times 10^{-3}$. Details on the analytical methods can be found in Qiu and Jiang (2007). Data were reduced using the ArArCALC software (Koppers, 2002).

Zircon was separated from one sample of the San Pelayo orthogneiss using magnetic and heavy-liquid techniques. Zircon grains were studied by cathodoluminescence imaging and analyzed for U-Th-Pb using the Cameca IMS-1280 ion microprobe of the NENIMPF facility in Woods Hole, Massachusetts, and the LA-ICPMS of the University of Granada. Details of the methods are given in Bea et al. (2006).

Additionally, 18 samples of low-grade metapelites from the SGC (see Bea et al., 2003) and 14 samples of metapelitic granulite xenoliths (5.5 to 8 kbar; Bea et al., 1999) scavenged by Early Permian lamprophyres (Scarrow et al., 2006) were analyzed for boron by prompt-gamma neutron activation analysis at McMaster University, Canada, following the method described by Shaw and Smith (1991).

RESULTS

Boron concentrations in upper crustal metapelites and lower crustal metapelitic xenoliths

The concentration of boron in the 18 low-grade metapelites from the SGC ranges from 14 to 78 ppm, with an average of 35 ppm and a standard deviation of 19 ppm (Table 1). These values match those reported by Pereira and Shaw (1997) for similar rocks of neighboring areas and may, therefore, be considered representative of Central Iberian metapelites. By contrast, the concentration of boron in the 14 metapelitic granulite xenoliths is about one order of magnitude lower. It ranges from 0.7 to 4.1 ppm with an average of 1.8 ppm and standard deviation of 0.9 ppm. U-Pb zircon data of the metapelitic xenoliths (Fernández-Suárez et al., 2006) reveal that their protolith consisted of materials similar to the low-grade metapelites and that they underwent several stages of metamorphism and anatexis during the Variscan. It seems, therefore, that during these episodes, the buried metapelites lost about 90% of the boron they originally contained.

Zircon ages

A total of 46 U-Th-Pb ion microprobe (12) and LA-ICPMS (34) determinations in 30 zircon grains separated from one sample of the San Pelayo orthogneiss revealed the situation characteristic of the Cambro-Ordovician magmatic rocks of Central Iberia, with several concordant or near concordant populations, from Cambro-Ordovician to Tomian and some, more discordant, grains with ages from Orosirian to Mesoarchean (Bea et al., 2006; Montero et al., 2007). The youngest concordant population corresponds to rims of zircon crystals (Fig. 3) and yielded a mean value of 207-corrected $^{238}U/2^{06}Pb$ age of 497 ± 5 Ma (at 95% confidence level). To discuss the meaning of the zircon distribution ages of the San Pelayo orthogneiss is beyond the scope of this work. Interested readers will find further information in the aforementioned articles. For our current purposes it is enough to know that the mean age of the youngest concordant population (496 ± 5 Ma) is considered to represent the crystallization age of the body.

$^{40}Ar/^{39}Ar$ ages

$^{40}Ar/^{39}Ar$ data for tourmaline analyses are summarized in Table 2; the raw dataset is included in the electronic supplementary material. Errors are reported at the 2 sigma level. The calculations of the plateau ages and MSWD were weighted according to the percentage of released ^{39}Ar in each step. The significance level was calculated with a $\chi 2$ test for n-1 degrees of freedom, where n is the number of steps and $\chi 2$ = MSWD * (n-1). The following stands out:

The age spectrum of the tourmaline from the San Pelayo orthogneiss yields a plateau at higher temperatures (Fig. 4A), which includes four steps and accounts for 57.2% of released ^{39}Ar. Its mean age is 370 ± 5 Ma, with a MSWD of 2.59 and a significance level of $\alpha = 0.052$. The apparent K/Ca (0.102 ± 0.003) is low and nearly constant. The normal and inverse isochron ages are 375 ± 13 Ma (MSWD = 0.6) and 373 ± 33 Ma with, in both cases, initial $^{40}Ar/^{36}Ar$ identical within error range to the atmospheric value (295.5). The plateau age of 370 ± 5 Ma, therefore, is statistically significant according to the most rigorous criterion (three or more consecutive steps accounting for more than 50% of released ^{39}Ar and $\alpha > 0.05$; e.g. Baksi, 2006).

The spectrum of this tourmaline also shows a pseudo-plateau at low-temperatures (Fig. 4A). It includes eight steps, accounting for a 38.3% of released ^{39}Ar, with a mean age of 342 ± 6 Ma (MSWD = 1.99) and a significance level of $\alpha = 0.052$. The apparent K/Ca clusters around 0.121 ± 0.01. The normal and inverse isochron ages are 336 ± 20 Ma (MSWD = 1.12) and 342 ± 19 Ma (MSWD = 2.2), close to the mean age defined by the pseudo-plateau. The initial $^{40}Ar/^{36}Ar$ of 312 ± 35 is within error range to the atmospheric value. Despite the pseudo-plateau accounts for less than 50% of released ^{39}Ar, the fact that it involves eight steps and has

TABLE 1 | **Major element (%) and borom (ppm) concentration of crustal metapelites and lower crustal xenoliths.**

id	SiO_2	TiO_2	Al_2O_3	$FeO^{tot.}$	MgO	MnO	CaO	Na_2O	K_2O	P_2O_5	B
upper crustal metapelites											
MP-1	58.32	0.85	20.18	8.19	1.79	0.05	0.17	0.87	3.9	0.32	46
MP-2	62.28	0.78	19.07	6.70	2.39	0.05	0.29	1.38	3.55	0.08	54
MP-3	52.96	0.66	20.88	9.83	0.61	0.02	0.12	0.15	4.97	0.07	14
MP-4	62.56	0.79	17.06	4.86	1.92	0.04	0.26	1.05	3.18	0.14	21
MP-5	61.28	0.80	21.07	2.39	2.56	0.04	0.21	1.51	4.23	0.03	39
MP-6	64.68	0.70	19.24	3.35	0.56	0.02	0.09	1.73	4.78	0.02	31
MP-7	63.18	0.40	16.57	4.86	3.15	0.06	1.81	1.96	3.09	0.80	18
MP-8	60.55	0.51	18.14	6.08	2.42	0.04	0.24	1.26	3.82	0.11	54
MP-9	72.73	0.73	10.48	2.98	1.40	0.06	3.32	2.76	1.46	0.10	37
MP-10	72.38	0.42	9.12	5.99	3.20	0.14	6.45	0.41	0.22	0.17	24
MP-11	71.70	0.39	11.22	4.84	1.71	0.10	7.72	0.38	0.78	0.16	19
MP-12	68.07	0.87	13.60	5.04	2.87	0.12	6.72	0.98	0.44	0.20	14
MP-13	80.36	0.59	6.02	4.01	1.93	0.10	4.31	0.57	0.55	0.25	78
MP-14	68.49	0.73	11.07	7.21	3.26	0.17	3.47	1.44	0.46	0.22	61
MP-15	75.08	0.21	10.11	4.91	1.52	0.13	5.77	0.37	0.26	0.12	22
MP-16	66.87	0.40	7.76	4.31	2.08	0.09	7.42	1.43	1.48	1.08	21
MP-17	67.34	0.83	13.36	6.49	2.26	0.08	1.89	4.4	0.82	0.18	15
MP-18	71.46	0.83	12.12	5.44	1.85	0.08	1.26	3.58	1.42	0.15	55
lower crustal xenoliths											
XE-1	64.22	0.94	17.22	7.43	3.51	0.09	0.97	1.64	3.6	0.13	0.7
XE-2	65.87	0.89	16.53	6.12	2.72	0.07	0.68	2.08	4.77	0.07	0.8
XE-3	61.79	0.93	16.75	8.62	3.89	0.11	0.97	1.13	4.25	0.17	0.9
XE-4	61.91	0.94	18.06	7.42	3.55	0.08	1.22	2.70	3.50	0.10	1.2
XE-5	67.63	0.83	16.5	4.85	2.57	0.08	1.67	2.60	2.24	0.06	1.4
XE-6	64.21	1.09	17.05	6.97	3.99	0.08	1.47	2.13	2.66	0.08	1.5
XE-7	62.05	0.80	18.44	6.28	3.40	0.11	2.29	2.99	2.86	0.26	1.6
XE-8	62.65	1.00	16.69	7.44	3.80	0.10	1.46	2.18	2.76	0.08	1.7
XE-9	64.59	0.77	16.87	6.80	3.17	0.08	1.14	1.87	3.81	0.12	1.9
XE-10	63.24	0.79	17.13	7.47	2.99	0.07	0.64	1.56	4.34	0.11	1.9
XE-11	65.33	0.88	15.29	6.58	3.04	0.09	1.76	2.10	3.19	0.13	2.1
XE-12	66.98	0.75	14.94	6.24	3.16	0.10	2.94	1.98	2.14	0.11	2.1
XE-13	68.16	0.78	15.12	5.49	2.74	0.09	3.44	1.80	1.93	0.10	3.2
XE-14	65.09	0.94	16.47	6.20	3.48	0.10	3.31	2.05	2.05	0.17	4.1

$\alpha > 0.05$ suggests that it may represent an event of argon loss at 342 ± 6 Ma.

The age spectrum of the mylonitized tourmalinite is intensely perturbed (Fig. 4B). Putting aside the first step, which has an excess of ^{40}Ar, the rest of the steps show a marked dispersion around 355 ± 13 Ma (see "plateau" I). These data, however, cannot be considered to define a plateau because the significance level is $\alpha < 0.0001$. If we instead consider just the 6 central steps, account for 44% of released ^{39}Ar, the mean age is 347 ± 9 Ma, with an MSWD = 3.48 and an improved, but still insufficient, significance level of $\alpha = 0.004$.

The step-heating spectrum from the folded tourmalinites is very similar to that of the mylonitized tourmalinite

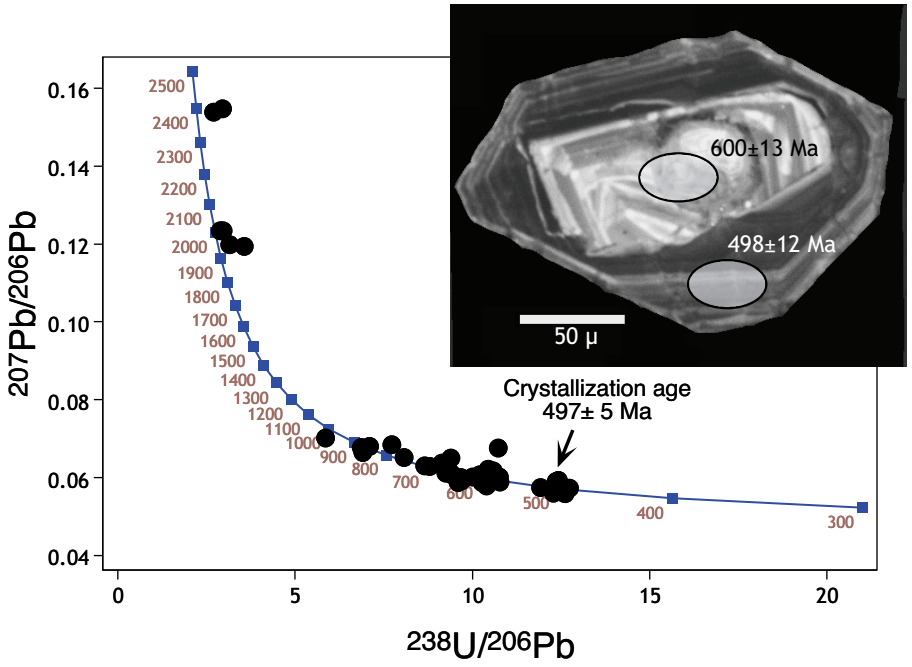

FIGURE 3 | **Tera-Wasserburg concordia plot for San Pelayo orthogneisses (raw data available from the authors and the Data Repository). The youngest concordant population represents the crystallization age at 496 ± 5 Ma, and mostly corresponds to euhedral rims over older cores (see inset). Remarkably, this rock contains Late Devonian tourmaline.**

(Fig. 4C): a first step with excess ^{40}Ar and 11 steps with apparent ages ranging from 303 to 361 Ma. Excluding the 303 Ma step, which is an outlier, the remaining ten steps yield an average of 342 ± 9 Ma with an MSWD of 21.47 and $\alpha < 0.0001$. This spectrum indicates that the sample is isotopically heterogeneous and it is not possible to estimate a precise age. However, the fact that their mean ages closely matches that of the low-temperature pseudo-plateau of the San Pelayo tourmaline gives additional support to the idea of an argon loss event at ca. 344 Ma.

The step-heating spectrum for the fine-banded tourmalinite is, however, totally different (Fig. 4D). The seven low-temperature steps out of a total of 11, accounting for a 78% of released ^{39}Ar yield a well-defined plateau age at 318 ± 2 Ma, with a low MSWD of 0.61 and = 0.722. The normal and inverse isochron ages are 322 ± 10 Ma and 321 ± 10 Ma, with initial $^{40}Ar/^{36}Ar$ of 275 ± 44 and 277 ± 30. The three high temperature steps yielded apparent ages from ca. 350 to 430 Ma and have distinctly lower apparent K/Ca.

The tourmaline disseminated in the metasediment yields a well-defined plateau age at 316 ± 2 Ma, with MSWD = 0.49 and $\alpha = 0.84$ (Fig. 4E). This plateau accounts for 95.1 % of released ^{39}Ar and includes all but the first and the last steps. The normal and inverse isochron ages are 314 ± 10 Ma and 313 ± 4 Ma, with MSWD of 0.12 and 0.17, and initial $^{40}Ar/^{36}Ar$ of 300 ± 21 and 303 ± 12 respectively. The inclusion of the last step (apparent age 335 ± 15 Ma) neither affects the mean age nor the statistical significance of the plateau, it simply increases the error on the mean.

Lastly, the tourmaline from the leucogranite yields a saddle-shaped $^{40}Ar/^{39}Ar$ age spectrum, with a minimum age of 296 Ma in the third step and ages around 323-326 Ma in the first and last steps. The mean age of the spectrum is 310 ± 5 Ma, with a MSWD of 6.94 and $\alpha < 0.0001$. This spectrum represents a isotopically heterogeneous sample, and although a mean age can be provided it would be geologically meaningless (e.g., Dallmeyer, 1979).

DISCUSSION

Considering field relations, petrographic observations and chemical data, Pesquera et al. (2005) proposed that the source of boron in the Martinamor Antiform was magmatic fluids derived from the crystallization of the San Pelayo granitoids, believed to be Ediacaran or Early Cambrian. These B-rich fluids would have metasomatized the metasediments of the Monterrubio Formation to produce pre-Variscan tourmalinites. Then, the late-Variscan anatexis involved the tourmalinites to produce B-rich crustal melts, the evolution of which caused the youngest generations of tourmaline-bearing rocks. However, the chronological data presented in this work suggest that there was no pre-Variscan tourmaline. Instead, different

TABLE 2 | **Summary of Ar-Ar ages.**

	San Pelayo orthogneiss		Milonitized tourmalinite		Folded tourmalinite	Fine-banded tourmalinite	Metasediment	Leucogranite
Plateau data								
age	Plateau I	Plateau II	Plateau I	Plateau II	Plateau I	Plateau I	Plateau I	Plateau I
number of steps	4	8	12	6	9	7	8	12
% ^{39}Ar released	57.2	38.3	94.9	44.0	94.9	78.0	95.1	100
Plateau age (Ma)	370 ± 5	344 ± 5	355 ± 13	347 ± 9	342 ± 9	318 ± 2	316 ± 2	310 ± 5
MSWD	2.59	1.99	17.84	3.48	21.47	0.61	0.49	6.94
α (from χ2 test)	0.051	0.052	<0.0001	0.004	<0.0001	0.722	0.84	<0.0001
Normal isochron								
age	375 ± 13	336 ± 20	322 ± 44	324 ± 69	338 ± 13	322 ± 10	314 ± 10	303 ± 13
$^{40}Ar/^{36}Ar$ initial	262 ± 80	312 ± 47	364 ± 95	346 + 150	301 ± 58	275 ± 44	300 ± 21	320 ± 49
MSWD	0.60	1.12	6.6	2.3	19	0.21	0.12	3.8
Inverse isochron								
age	373 ± 33	342 ± 19	312 ± 48	319 ± 61	338 ± 13	321 ± 7	313± 4	307 ± 9
$^{40}Ar/^{36}Ar$ initial	273 ± 230	300 ± 53	385 ± 110	359 ± 130	300 ± 67	277 ± 30	303 ± 10	307 ± 45
MSWD	4.6	2.2	9.2	2.9	15	0.48	0.17	7.5
Other data								
Total fusion age	361 ± 2		446 ± 4		367 ± 2	332 ± 2	315 ± 2	310 ± 2
J	0.011102		0.011155		0.011194	0.011138	0.011170	0.011118
J error (%)	0.15		0.15		0.15	0.15	0.15	0.15
apparent K/Ca	0.102 ± 3	0.121 ± 10	0.229 ± 19	0.242 ± 18	0.333 ± 20	0.258 ±90	0.051 ± 3	0.173 ± 6

Raw data are available as supplementary electronic material in http://earthref.org/cgi-bin/er.cgi?s=erda.cgi?n=811

generations of tourmalinites and tourmaline-bearing rocks were sequentially formed from the beginning to the end of the Variscan history of this region.

The protoliths of the San Pelayo orthogneisses are indeed pre-Variscan, with a precise zircon crystallization age of 496 ± 5 Ma. The question is, therefore, to find out whether the 370 ± 5 Ma plateau of their resident tourmaline represents a primary crystallization age or was caused by resetting of Cambrian tourmaline. Our data indicate that the first alternative is more likely. First, because the plateau corresponds to the high-temperature part of the spectrum, is statistically significant and involves more than 50% of released ^{39}Ar. Second, because it appears that there is no evidence for any ca. 370 Ma event capable of fully resetting the tourmaline,

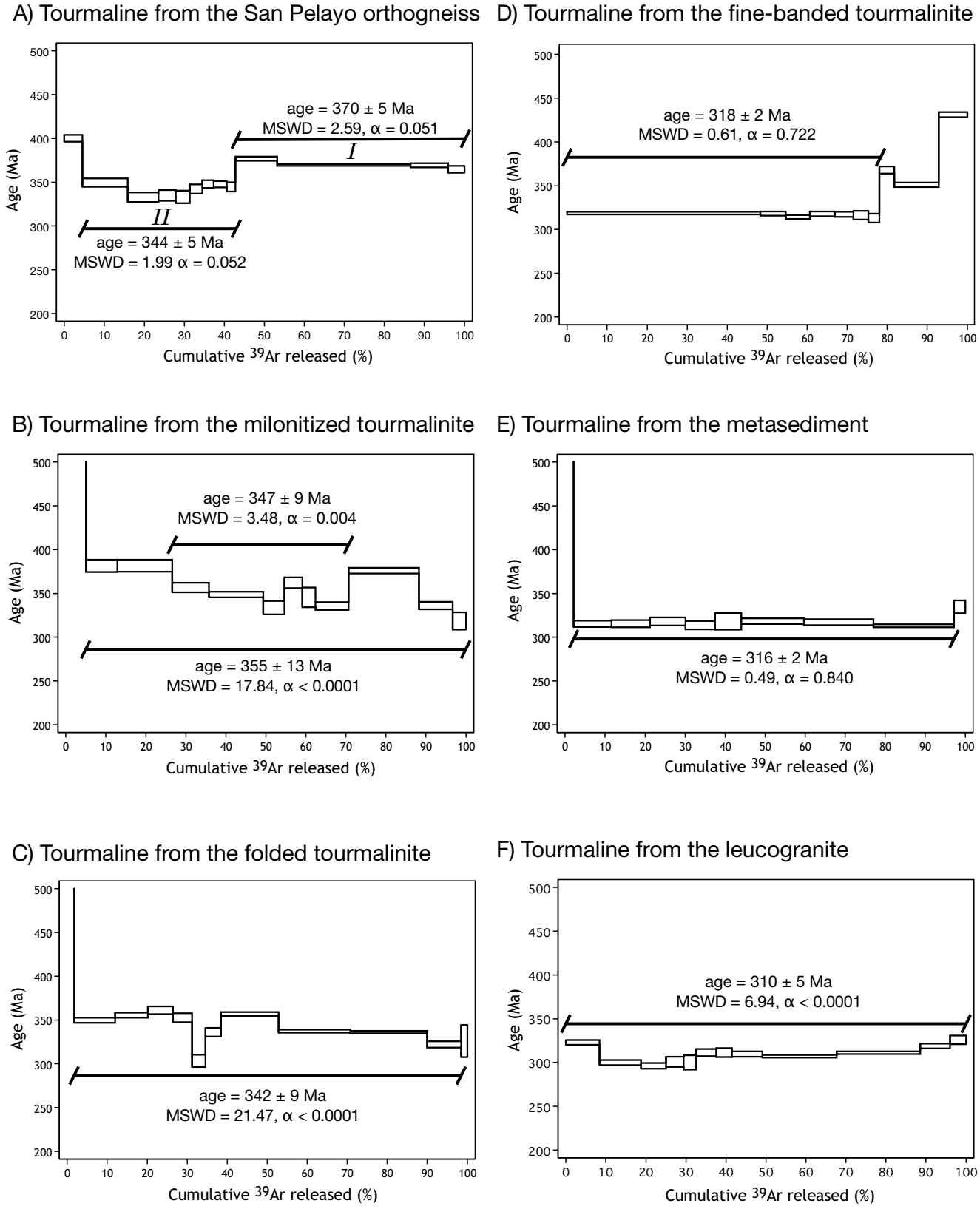

FIGURE 4 | **$^{40}Ar/^{39}Ar$ release patterns of the 6 samples studied. See text for discussion. Raw data and isochrons are available from the authors and the Data Repository.**

which according to Andriessen et al. (1991) has an Ar closure temperature probably exceeding that of hornblende (~550 °C). Indirect evidence for the elevated Ar retentiveness of tourmaline could be inferred from the preservation in the San Pelayo tourmaline of ages older that the thermal peak of the Variscan metamorphism, which in Central Iberia occurred at 332-335 Ma (Montero et al., 2004).

However, apparent ages older than accurately dated geological events are a common feature of different minerals in metamorphic terranes. They can result from excess argon incorporation. Excess argon is normally seen as saddle-shaped age spectrum, but it may also produce linear arrays on $^{36}Ar/^{40}Ar$ *vs*. $^{39}Ar/^{40}Ar$ correlation diagrams, leading to geologically meaningless plateau ages that are older than the true closure age (e.g., Arnaud and Kelly, 1995). Therefore, there is no unambiguous evidence for elevated Ar retentiveness of the tourmaline.

Accordingly, it is likely that the 370 ± 5 Ma plateau represents the age of crystallization of primary tourmaline in the ca. 496 Ma San Pelayo orthogneiss rather than resetting of Cambrian tourmaline. For this reason, this tourmaline would be metasomatic, approximately coeval with the formation age of the S1 fabrics. To ascertain why the gneisses underwent boron metasomatism at 370 Ma, we have two lines of evidence. First, the different concentration of boron in upper-crustal metapelites (35 ± 19 ppm) and low-crustal metapelitic xenoliths (1.9 ± 0.9 ppm) suggests that metapelites displaced to the lower crust because of crustal stacking have suffered an intense boron depletion. Second, this date coincides (see Fig. 5) with 1) the age of the first deformation phase in other regions of Iberia, for example with the oldest $^{40}Ar/^{39}Ar$ age recorded by amphibole inside the Coimbra-Badajoz-Córdoba Shear Zone (CBC, Fig 1) (370-360 Ma; Quesada and Dallmeyer, 1994), supposed to be root zone of the Central Iberian nappes (Matte, 2001); 2) with the $^{40}Ar/^{39}Ar$ age of D1 (365-370 Ma) determined in the Malpica-Tuy unit of NW Spain by Rodríguez et al. (2003), albeit slightly older than reported in muscovites developed associated with D1 in the OS Domain (ca. 359 Ma, Dallmeyer et al., 1997) (Fig 5).

When all these points are considered together, it seems reasonable to assume that boron was extracted by fluids released by dehydration reactions upon progressive heating as metapelites were buried (e.g., Leeman et al., 1992; Moran et al., 1992; Leeman and Sisson, 1996). Since boron in magmatic-hydrothermal systems is partitioned in the highly mobile water-vapor phase preferentially over melts and brines (Schatz et al., 2004), the hydrous B-rich fluids would have percolated fast to upper crustal levels, especially if the crust was suffering simultaneous deformation, with tourmaline precipitating wherever the environmental conditions permitted. The isotope composition of boron in tourmaline from the tourmalin-

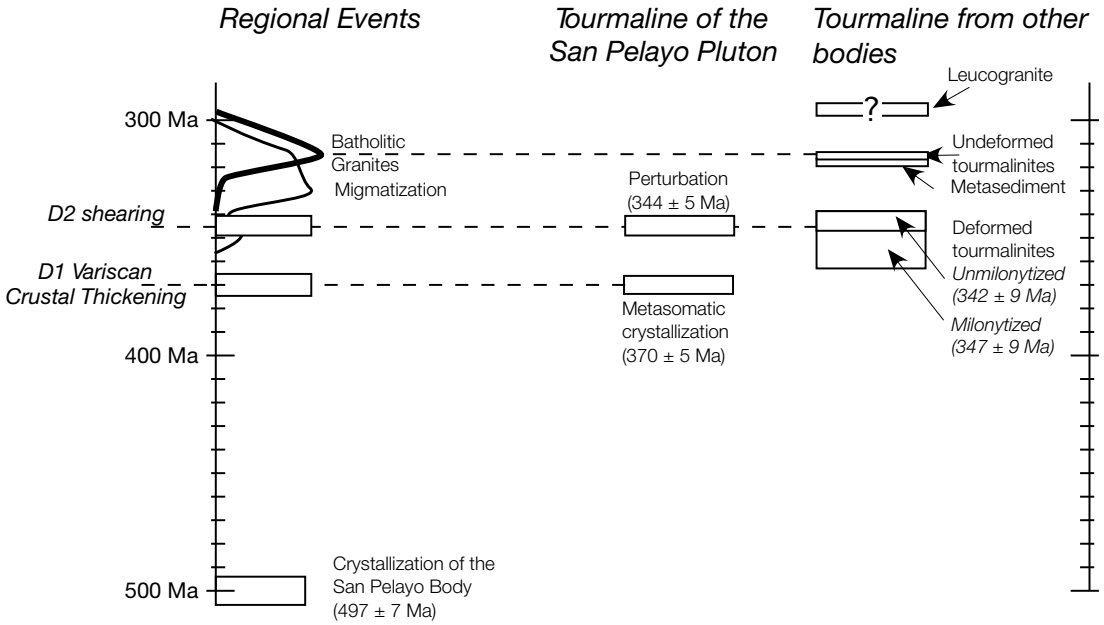

FIGURE 5 | **Correlation between $^{40}Ar/^{39}Ar$ ages of tourmaline and regional events. $^{40}Ar/^{39}Ar$ ages of the Coimbra-Badajoz-Córdoba (CBC) Shear Zone are from Quesada and Dallmeyer (1994), D1 in the Galicia Tras-os-Montes Zone from Rodríguez et al. (2003), D1 and D2 in the OS-Domain from Dallmeyer et al. (1997), zircon ages of migmatites are from Montero et al. (2004), and the ages of granites are from Bea et al. (1999). Note how the two main deformation phases, D1 and D2, are reflected by two generations of tourmaline formation.**

ites ($\delta^{11}B$ -4.4‰ to 2.2‰; Pesquera et al., 2005) being consistent with a provenance from metasediments, gives additional support to this idea. For these reasons, we propose that the tourmaline of the San Pelayo orthogneisses was formed during the initial stages of crustal thickening, and that the 370 ± 5 Ma plateau age represents, therefore, the closest radiometric estimate currently available for the Variscan crustal thickening in the SGC Domain of Central Iberia.

The second plateau of the San Pelayo tourmaline at 344 ± 5 Ma apparently represents an episode of Ar loss. Considering that it coincides (Fig. 5) with the age of the neighboring Cespedosa leucogranite (ca. 344 ± 5 Ma, Bea et al., 1999), which is syntectonic with the second main phase of Variscan deformation (D2), and with the age of muscovites associated with S2 (ca. 343 Ma, Dallmeyer et al., 1997), we propose that the Ar loss reflected by the plateau occurred as a consequence of the milonitization caused by the second main Variscan deformation phase (D2). The mean ages of the mylonitized (347 ± 9 Ma) and folded (342 ± 9 Ma) tourmalinites may also be related to D2 by two possible mechanisms: by either partial or total resetting of older tourmaline or by the formation of new tourmaline due to focused boron metasomatism along D2 shear zones. The feasibility of the first mechanism is revealed by the plateau II of the San Pelayo orthogneisses and seems to be a consequence of the intracrystalline deformation and recrystallization (Figs. 2B, C, B) caused by D2 shear zones. The second mechanism is suggested by the fact that tourmalinites located in shear zones are often not mylonitized, simply folded with little or no grain-size reduction.

The tourmaline from the fine-banded tourmalinite and the metasediment yielded well defined plateaus at 318 ± 2 Ma and 316 ± 2 Ma (Fig. 4D and E) which reveal the formation of primary tourmaline at that time. In the first case, the plateau does not include the last three steps, which account for 22% of released ^{39}Ar, with ages in the range 351-431 Ma. Accordingly, the low-temperature plateau could be interpreted as partial resetting of an older tourmaline. Nevertheless, the plateau flatness (strongly contrasting with the roughness of the age spectra shown in Fig. 4A and B), the age similarity between plateau and isochron ages, as well as the similar age to the plateau of the tourmaline from the metasediment (which can rightly be considered to represent a crystallization age), suggest that younger and volumetrically more important rims overgrew around older cores of tourmaline.

As indicated by Pesquera et al. (2005), the tourmaline crystallized at 318-316 Ma was a product of recycling of the older tourmaline, caused by the Late Variscan granite activity of this area, which peaked at that time (Bea et al., 2003) (Fig. 5). The stability of tourmaline in low-pressure anatexites is limited by dehydration (Von Goerne et al., 1999) or melting reactions (Kawakami, 2001) which occur at ~700 °C. This temperature has been exceeded in the neighboring anatectic complexes (Pereira, 1998) so that any tourmaline present in their protoliths would have broken down, concentrating the released boron into the anatectic melts. Any water-rich vapor phase exsolved during the crystallization of these melts would have been strongly enriched in boron (Schatz et al., 2004) and, therefore, likely to precipitate metasomatic tourmaline, either focussed or dispersed, during migration to lower P T regions.

Lastly, the tourmaline separated from the leucogranite yields a saddle-shaped spectrum with a mean age of 310 ± 5 Ma, which probably indicates excess ^{40}Ar (Lanphere and Dalrymple, 1976). The spectrum begins at ~323 Ma, reaches a minimum at 296 Ma in the first step, and then increases until 326 Ma in the last step. Accepting that there is excess ^{40}Ar, the minimum value of 296 Ma would approach, but probably not reach, the real age of the rock. Therefore, the leucogranite could be related to the youngest granite magmatism of this sector of the Avila batholith, which is tourmaline-bearing and has ages clustering at 295 Ma (Bea et al., 1994; 1999).

CONCLUSIONS

Tourmaline appeared in the geological history of the Martinamor Antiform as a consequence of the crustal stacking caused by the Variscan collision. The metapelites displaced to the lower crust were intensely depleted in boron, the concentration of which decreased from ~35 ppm to ~1.9 ppm. Boron was extracted by fluids released by dehydration reactions upon progressive heating and concentrated in the water-vapor phase. Then these B-rich fluids quickly percolated upwards through the deforming crust to precipitate tourmaline wherever the environmental conditions permitted. The crystallization age of 370 ± 5 Ma of the tourmaline of the San Pelayo orthogneisses (plateau I, Fig. 4) would represent the age of this event and is, therefore, the closest radiometric estimate currently available for the Variscan crustal thickening in the Central Iberian Zone.

The age of 344 Ma recorded by tourmaline of the San Pelayo orthogneisses (plateau II, Fig. 4) and by the mylonitized and folded tourmalinites is thought to be related to D2. In most cases, it represents an episode of Ar loss triggered by intense mylonitization of tourmaline. It is also probable that it might represent the formation of new tourmaline due to focused boron metasomatism along D2 shear zones.

After the metamorphic peak and coinciding with the episode of maximum granite activity in the neighboring Avila batholith, a new generation of tourmaline (318-316 Ma) appeared either in fine-banded, undeformed tourmalinites or disseminated within Cambrian-Ediacaran metasediments. This stage of tourmalinitization was a consequence of the involvement of older tourmaline in the Variscan anatexis. The age of the last generation of tourmaline could not be determined precisely because it contained some ^{40}Ar excess, but it is probably around 295 Ma, coincident with the youngest Variscan granite magmatism in the area.

Though further work is required, our results suggest that tourmaline is an excellent chronological marker of deformation and magmatism in orogens that involved materials with water-soluble boron species. This mineral seems suitable for obtaining accurate results using the $^{40}Ar/^{39}Ar$ method because it combines an elevated Ar retentiveness and, at least in the samples studied here, little tendency to have ^{40}Ar excess.

ACKNOWLEDGEMENTS

We thank Andrey V. Korsakov and an anonymous reviewer for their constructive comments. We are also grateful to Jane H. Scarrow for her help with the English. This work has been supported by the Spanish grants CGL2006-07938 and CLG2005-05863, and the Andalucian grant RNM1595.

REFERENCES

Allen, P., 1991. Provenance research; Torridonian and Wealden. In: Morton, A.C., Todd, S.P., Haughton, P.D.W. (ed.). Developments in sedimentary provenance studies. Geological Society Special Publications, 57, 13-21.

Andriessen, P.A.M., Hebeda, E.H., Simon, O.J., Verschure, R.H., 1991. Tourmaline K-Ar ages compared to other radiometric dating systems in Alpine anatectic leucosomes and metamorphic rocks (Cyclades and Southern Spain). Chemical Geology, 91, 33-48.

Anglin, C.D., Jonasson, I.R., Franklin, J.M., 1996. Sm-Nd dating of scheelite and tourmaline: Implications for the genesis of Archean gold deposits, Val d'Or, Canada. Economic Geology, 91, 1372-1382.

Arnaud, N.O. and Kelley, S.P., 1995. Evidence for excess argon during high pressure metamorphism in the Dora Maira Massif (western Alps, Italy), using a ultra-violet laser ablation microprobe ^{40}Ar-^{39}Ar technique. Contributions to Mineralogy and Petrology, 121, 1-11.

Azor, A., Expósito, I., González Lodeiro, F., Simancas, J.F., Martínez Poyatos, D., 2004. Propuesta de un modelo evolutivo para la Zona de Ossa Morena. In: Vera, J.A. (ed.). Geología de España, Madrid, SGE-IGME, 188-189.

Baksi, A.J., 2006. Guidelines for assesing the reliability of $^{40}Ar/^{39}Ar$ plateau ages: Application to ages relevant to hotspot tracks. http://www.mantleplumes.org/ArAr.html.

Bea, F., Montero, P., Molina, J.F., 1999. Mafic precursors, peraluminous granitoids, and late lamprophyres in the Avila batholith: A model for the generation of Variscan batholiths in Iberia. Journal of Geology, 107, 399-419.

Bea, F., Montero, P., Talavera, C., Zinger, T., 2006. A revised Ordovician age for the oldest magmatism of Central Iberia: U-Pb ion microprobe and LA-ICPMS dating of the Miranda do Douro orthogneiss. Geologica Acta, 4, 395-401.

Bea, F., Montero, P., Zinger, T., 2003. The Nature and Origin of the Granite Source Layer of Central Iberia: Evidence from Trace Element, Sr and Nd Isotopes, and Zircon Age Patterns. Journal of Geology, 111, 579-595.

Bea, F., Pereira, M.D., Corretgé, L.G., Fershtater, G.B., 1994. Differentiation of strongly peraluminous, perphoshorous granites. The Pedrobernardo pluton, central Spain. Geochimica et Cosmochimica Acta, 58, 2609-2628.

Chen, C.H., Depaolo, D.J., Lan, C.Y., 1996. Rb-Sr microchrons in the Manaslu granite: Implications for Himalayan thermochronology. Earth and Planetary Science Letters, 143, 125-135.

Dallmeyer, R.D., 1979. $^{40}Ar/^{39}Ar$ Dating: Principles, Techniques, and Applications in Orogenic Terranes. In: Jaeger, E., Hunziker, J.E. (eds.). Springer-Verlag, Berlin, Lectures in Isotope Geology, 77-105.

Dallmeyer, R.D., Catalan, J.R.M., Arenas, R., Ibarguchi, J.I.G., Alonso, G.G., Farias, P., Bastida, F., Aller, J., 1997. Diachronous Variscan tectonothermal activity in the NW Iberian Massif: Evidence from $^{40}Ar/^{39}Ar$ dating of regional fabrics. Tectonophysics, 277, 307-337.

Díaz Montes, A., Navidad, M., González Lodeiro, F., and Martínez Catalán, J.R., 2004. El Ollo de Sapo. In: Vera, J.A. (ed.). Geología de España, Madrid, SGE-IGME, 69-72.

Díez Balda, M.A., 1986. El Complejo Esquisto-Grauwáckico, las series Paleozoicas, y la estructura Hercínica al sur de Salamanca. Salamanca, Ediciones Universidad de Salamanca, 162 pp.

Díez Balda, M.A., Martínez Catalán, J.R., Ayarza, P., 1995. Syncollisional extensional collapse parallel to the orogenic trend in a domain of steep tectonics: The Salamanca Detachment Zone (Central Iberian Zone, Spain). Journal of Structural Geology, 17, 163-182.

Fernández-Suárez, J., Arenas, R., Jeffries, T.E., Whitehouse, M., Villaseca, C., 2006. A U-Pb Study of Zircons from a Lower Crustal Granulite Xenolith of the Spanish Central System: A Record of Iberian Lithospheric Evolution from the Neoproterozoic to the Triassic. Journal of Geology, 114, 471-484.

Fitch, F.J., Miller, J.A., 1972. $^{40}Ar/^{39}Ar$ dating of detrital tourmaline and tourmalinized rocks; schists and micas. Journal of the Geological Society of London, 128, 291-294.

Frei, R., Pettke, T., 1996. Mono-sample Pb-Pb dating of pyrrhotite and tourmaline: Proterozoic vs Archean intracratonic gold mineralization in Zimbabwe. Geology, 24, 823-826.

Frei, R., Pettke, T., 1997. Mono-sample Pb-Pb dating of pyrrhotite and tourmaline: Proterozoic vs. Archean intracratonic gold mineralization: Reply. Geology, 25, 670-671.

Kawakami, T., 2001. Tourmaline breakdown in the migmatite zone of the Ryoke metamorphic belt, SW Japan. Journal of metamorphic Geology, 19, 61-75.

Koppers, A.A.P., 2002. ArArCALC - software for $^{40}Ar/^{39}Ar$ age calculations. Computers and Geoscience, 28, 605-619.

Kudryashov, N.M., Gavrilenko, B.V., Apanasevich, E.A., 2004. U-Pb, Pb-Pb tantalite and tourmaline dating of rare metal pegmatites from the Kolmozero-Voron'ya greenstone belt (NE Baltic Shield). Geochimica et Cosmochimica Acta, 68, A678-A678.

Lanphere, M.A., Dalrymple, G.B., 1976. Identification of excess ^{40}Ar by the $^{40}Ar/^{39}Ar$ age spectrum technique. Earth and Planetary Science Letters, 32, 141-148.

Leeman, W.P., Sisson, V.B., 1996. Geochemistry of boron and its implications for crustal and mantle proceses. In: Grew, E.S., Anovitz, L.M. (eds.). Boron: Mineralogy, petrology and geochemistry. Reviews in Mineralogy, 33, 645-707.

Leeman, W.P., Sisson, V.B., Reid, M.R., 1992. Boron geochemistry of the lower crust: Evidence from granulite terranes and deep crustal xenoliths. Geochimica et Cosmochimica Acta, 56, 775-788.

Martínez Catalán, J.R., Poyatos, D., Bea, F. (coordinators), 2004. La Zona Centroibérica. In: Vera, J.A. (ed.). Geología de España, Madrid, SGE-IGME, 68-133.

Matte, P., 2001. The Variscan collage and orogeny (480-290 Ma) and the tectonic definition of the Armorica microplate: a review. Terra Nova, 13, 122-128.

Montero, P., Bea, F., González-Lodeiro, F., Talavera, C., Whitehouse, M., 2007. Zircon crystallization age and protolith history of the metavolcanites and metagranites of the Ollo de Sapo Domain in central Spain. Implications for the Neoproterozoic to Early-Paleozoic evolution of Iberia. Geological Magazine, 144, 963-976.

Montero, P., Bea, F., Zinger, T.F., Scarrow, J.H., Molina, J.F., Whitehouse, M.J., 2004. 55 Million Years of Continuous Anatexis in Central Iberia: Single Zircon Dating of the Peña Negra Complex. Journal of the Geological Society, 161, 255-264.

Moran, A.E., Sisson, V.B., Leeman, W.P., 1992. Boron depletion during progressive metamorphism: Implications for subduction processes. Earth and Planetary Science Letters, 111, 331-349.

Pereira, M.D., 1998. P-T conditions of generation of the Pena Negra anatectic complex, central Spain. Petrology, 6, 555-563.

Pereira, M.D., Shaw, D.M., 1997. Behaviour of boron in the generation of an anatectic complex: The Peña Negra complex, central Spain. Lithos, 40, 179-188.

Pesquera, A., Torres-Ruiz, J., Gil-Crespo, P.P., Jiang, S.Y., 2005. Petrographic, chemical, and B-isotopic insights into the origin of tourmaline-rich rocks and boron recycling in the Martinamor antiform (Central Iberian Zone, Salamanca, Spain). Journal of Petrology, 46, 1013-1044.

Pesquera, A., Velasco, F., 1997. Mineralogy, Geochemistry and geological significance of tourmaline-rich rocks from the Paleozoic Cinco Villas massif (western Pyrenees, Spain). Contributions to Mineralogy and Petrology, 129, 53-74.

Qiu, H.N., Jiang, Y.D., 2007. Sphalerite $^{40}Ar/^{39}Ar$ progressive crushing and stepwise heating techniques. Earth and Planetary Science Letters, 256, 224-232.

Quesada, C., Dallmeyer, R.D., 1994. Tectonothermal evolution of the Badajoz-Córdoba shear zone (SW Iberia): characteristics and $^{40}Ar/^{39}Ar$ mineral age constraints. Tectonophysics, 231, 195-213.

Richards, J.P., Wagner, P.A., 1997. Mono-sample Pb-Pb dating of pyrrhotite and tourmaline: Proterozoic vs. Archean intracratonic gold mineralization: Comment. Geology, 25, 669-670.

Rodríguez, J., Cosca, M.A., Gil Ibarguchi, J.L., Dallmeyer, R.D., 2003. Strain partitioning and preservation of $^{40}Ar/^{39}Ar$ ages during Variscan exhumation of a subducted crust (Malpica - Tui complex, NW Spain). Lithos, 70, 111-139.

Scarrow, J., Bea, F., Montero, P., Molina, J.F., Vaugham, A.P.M., 2006. A precise $^{40}Ar/^{39}Ar$ age for Central Iberian camptonitic lamprophyres. Geologica Acta, 4, 451-460.

Schatz, O.J., Dolejs, D., Stix, J., William-Jones, A.E., Layne, G.D., 2004. Partitioning of boron among melt, brine and vapor in the system haplogranite-H_2O-NaCl at 800 °C and 100 MPa. Chemical Geology, 210, 135-147.

Shaw, D.M., Smith, P. L., 1991. Concentration of B, Sm, Gd, and H in 24 reference materials. Geostandards Newsletters, 15, 59-66.

Simancas, J.F., Carbonell, R., González Lodeiro, F., Pérez Estaún, A., Juhlin, C., Ayarza, P., Kashubin, A., Azor, A., Martínez Poyatos, D., Almodóvar, G.R., Pascual, E., Sáez, R., Expósito, I., 2003. The Crustal Structure of the Transpressional Variscan Orogen of SW Iberia: The IBERSEIS Deep Seismic Reflection Profile. Tectonics, 22(6), 1-16. DOI: 10.1029/2002TC001479.

Villa, I.M., 1990. Geochronology and excess Ar geochemistry of the Lhotse Nup leucogranite, Nepal-Himalaya. Journal of Volcanology and Geothermal Research, 44, 89-103.

Villaseca, C., Downes, H., Pin, C., Barbero, L., 1999. Nature and composition of the lower continental crust in central Spain and the granulite-granite linkage: Inferences from granulitic xenoliths. Journal of Petrology, 40, 1465-1496.

Von Goerne, G., Franz, G., Robert, J.L., 1999. Upper thermal stability of tourmaline plus quartz in the system MgO-Al_2O_3-SiO_2-B_2O_3-H_2O and Na_2O-MgO-Al_2O_3-SiO_2-B_2O_3-H_2O-HCl in hydrothermal solutions and siliceous melts. Canadian Mineralogist, 37, 1025-1039.

Wijbrans J.R., Pringle M.S., Koppers, A.A.P., Scheveers R., 1995. Argon Geochronology of Small Samples Using the Vulkaan Argon Laserprobe. Proceedings Koninklije Nederlandse Akademie van Wetenschappen, Biological, Chemical, Geological, Physical and Medical Sciences, 98, 185-218.

Manuscript received March 2008;
revision accepted October 2008;
published Online September 2009.